

Online Shaping for ISI Channels with a Limited Number of ADC Bits

Or Levi
Dept. of EE-Systems, TAU
Tel-Aviv, Israel
Email: orl1@mail.tau.ac.il

Dan Raphaeli
Dept. of EE-Systems, TAU
Tel-Aviv, Israel
Email: danr@eng.tau.ac.il

Abstract—An online shaping technique for high performance communication over Gaussian channels with Inter-Symbol Interference (ISI) and receiver Analog to Digital Converter (ADC) noise is presented. The technique uses online transmitter precoding over Pulse Amplitude Modulation (PAM) constellation, designed to shape the symbols distribution so that peak power constraint at the channel output is satisfied. An iterative decoder shares information between a modified M-BCJR module, which computes online the trellis transition probabilities of the shaped distribution, and turbo decoder. The result is a reduction in the required ADC Effective Number Of Bits (ENOB), which is in particular attractive in modern high-speed wireline links. Theoretical bounds are analytically derived which enable to assess the possible gain using shaping. On practical scenarios aim to transmit 200 Gbps and 400 Gbps over printed circuit board, we demonstrate in simulations an overall ENOB gains as high as 1.43 bit and 1.78 bit, respectively, compared to uniform 4-PAM transmission with turbo equalization at the receiver side.

I. INTRODUCTION

The ever increasing demand for higher data rates in wireline communication links imposes the use in sophisticated digital equalization techniques, usually implemented at the receiver side [1]. Those, require using high-speed front-end ADCs for proper analog to digital signal conversion.

It is well-known that a major non-ideal issue of wireline links is the frequency dependent channel loss. Such a behaviour causes an increment in both ISI and PAPR of the signal at the channel output as baud rate increases. To avoid excessive signal distortion due to clipping the ADC is required to supply large dynamic range, which leads to high ENOB [2] requirement to achieve the desired system performance. The demand of large dynamic range translates to higher circuit design complexity and higher power consumption, which are among the key issues in high-speed applications.

Fischer proposed Dynamics Limited Precoding (DLP) technique [3] that allows receiver PAPR control. DLP is an extension of the well-known Tomlinson-Harashima Precoder (THP) [4], which offers a trade-off between transmitter and receiver PAPR. One extreme point of DLP is original THP, with minimal PAPR at channel input and maximal PAPR at channel output. The other extreme point is essentially channel inversion at the transmitter which provides minimal PAPR at channel output in expense of maximal PAPR at channel input. Since channel input (transmitter output) is voltage limited and

quantization prone due to the Digital to Analog Converter (DAC), DLP shifts the problem to the transmitter side without providing any gain overall. On the contrary, the quantization noise at the transmitter is an additional noise source.

A common equalizer that can be used for ISI (and PAPR) reduction at the ADC input is a Continuous Time Linear Equalizer (CTLE) [5]. CTLE has several disadvantages. First, CTLE introduces large impedance discontinuity at the channel and equalizer interface. Impedance matching networks, often employ inductors, can be used to prevent the discontinuity. However, the large inductors make this approach less suitable for on-chip integration. In addition, CTLE must be optimized for each channel and both devising adaptation algorithm and practically modifying the components at high frequencies are formidable challenges.

Inspired by the mathematical similarity between the problem at hand and the problem of PAPR reduction at the transmitter due to the pulse shaping filter effect, we sought to derive a parallel technique. A recent shaping technique for PAPR reduction at the transmitter was presented in [6]. To avoid peak excursions at the pulse shaping filter output, symbol transitions which result in high peak values are removed from the trellis graph, so that PAPR gain is achieved compared to un-shaped transmission. However, both implementation and theoretical analysis require a prior calculation of the shaped distribution which is stored in a table. The table size depends exponentially on the pulse shape filter span. Hence, it cannot be used for practical long channels due to the enormous size of the required memory.

In this paper, we propose an online shaping scheme for PAPR reduction at the output of wireline channels that enables to reduce the ADC ENOB requirement compared to un-shaped transmission. By theoretical analysis we derive an upper-bound on the shaping gain and we show that the proposed scheme approaches it. The shaping scheme is attractive especially in high-speed links due to high PAPR at the ADC input on the one hand, but limited receiver power consumption and complexity on the other hand. Whereas [6] requires high memory and a prior calculation of the shaped distribution, the proposed shaping scheme is designed to eliminate these demands by employing online calculation of the distribution (both at transmitter and receiver). It can therefore be used for

practical long channels. Since the suggested shaping scheme uses transmitter precoding over a standard PAM constellation, and does not use any filter, then, unlike transmitter equalization and DLP it does not increase either transmitter PAPR or number of signal levels at the transmitter. Therefore, it has no effect on the required transmitter hardware (e.g., DAC and power amplifier). For data rates 200 Gbps and 400 Gbps, a shaped 8-PAM transmission achieves ADC ENOB gains of 1.43 bit and 1.78 bit, respectively, compared to uniform 4-PAM transmission with Turbo-Equalizer (TE) [7] at the receiver.

The rest of the paper is organized as follows: Section II describes the system model. In Section III we present the on-line shaping process, both for the Tx and Rx parts. In Section IV we present a theoretical analysis and derive the achievable gains using shaping. Section V presents simulation results of the shaped system, compared to a uniform transmission. In Section VI conclusion remarks are given.

II. SYSTEM MODEL

A typical communication link may be adequately described by the model shown in Fig. 1. Let $\mathbf{X} = (-Q + 1, -Q + 3, \dots, Q - 3, Q - 1)$ be one dimensional Q -PAM constellation with cardinality $|\mathbf{X}| = Q$, and let $x^N \triangleq (x_0, \dots, x_{N-1})$ be

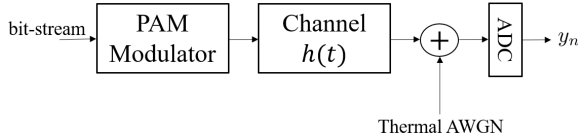


Figure 1: System model.

a frame of N symbols where $x_n \in \mathbf{X} \forall n$. The frame x^N is transmitted in symbol rate f_s symbols/sec through a noisy channel with an impulse response $h(t)$ and sampled by ADC every $1/f_s$ seconds. The resulting sampled signal at the ADC output is given by

$$y_n = \sum_{i=0}^{L-1} h_i x_{n-i} + z_n + \eta_n = r_n + z_n + \eta_n \quad (1)$$

where z_n and η_n are two independent sources of one dimensional white Gaussian noise with variance $N_0/2$ and $N_A/2$, respectively, L is the channel span in symbol periods units, and $r_n = \sum_{i=0}^{L-1} h_i x_{n-i}$ is the sampled signal at the n -th time step. The noise z_n is receiver thermal noise and η_n is additional noise caused by the ADC as a result of the quantization process and distortion, approximated as AWGN. This approximation is justified since quantization noise in practical ADCs rarely have uniform quantization noise. The noise in practical ADCs is influenced by inaccuracies, non-linearities, clock jitter, and thermal noise inside ADC which overall can be approximated as white gaussian noise sources [8].

The instantaneous power of the received signal is $p_n = |r_n|^2$ and the Signal to Noise Ratio (SNR) is defined by (2) where $P_r = E\{p_n\}$ is the average power of the signal, and $E\{\cdot\}$ denotes the statistical averaging.

$$SNR \triangleq \frac{2P_r}{N_A + N_0} \quad (2)$$

The PAPR at the ADC input is the ratio between the peak power p_{peak} and the average power P_r , where p_{peak} is defined as the value of p_n which is exceeded with probability ϵ . In this paper we use $\epsilon = 10^{-4}$. In addition, we normalized constellation points so that average uniform transmission power is 1.

The Signal to Noise and Distortion Ratio (SNDR) and the ENOB of an ADC device are defined by [2]

$$SNDR \triangleq \frac{2P_r}{N_A} \quad (3)$$

$$ENOB \triangleq \frac{10 \cdot \log_{10}(SNDR \cdot PAPR) - 4.76}{6} \quad (4)$$

Since shaping for PAPR reduction allows an equivalent increment in the average power of the received signal, the overall shaping gain G_T is the sum of the PAPR and SNDR gains (if denoted in dB), given constant ratio between the transmitted average power $P_t = E\{|x_n|^2\}$ and thermal noise N_0 . This ratio is denoted by Transmitter Signal to Thermal Noise Ratio (TSTNR).

A typical wireline channel, with a causal continuous time impulse response, could be approximated as [9]

$$h(t) = \frac{A}{\sqrt{(t_0 + t)^3 e^{\frac{\pi A^2}{t_0 + t}}}} \otimes \frac{2B}{\pi((t_0 + t)^2 + B^2)}, t \geq 0 \quad (5)$$

where A and B are positive constants that determine the relaxation time of the response and $t_0 \geq 0$ is a parameter that determines the first sample of $h(t)$. In this paper, we use $t_0 = 7.7 \cdot 10^{-13} \text{sec}$, $A = 10^{-6} \sqrt{\text{sec}}$ and $B = 8.8 \cdot 10^{-12} \text{sec}$, which are typical values of a microstrip trace of length 50 cm used for communicating between two chips [9]. The discrete sampled impulse response is therefore $h_n = h(t_0 + n/f_s)$. The symbol rates we use in this paper are $f_s = 112 \text{Gsymb/sec}$ and $f_s = 224 \text{Gsymb/sec}$. The resulting voltage gain normalized sampled impulse responses are

$$h_A = \{0.13, 0.19, 0.14, 0.09, 0.07, 0.05, 0.037, 0.031, 0.025, 0.02, 0.016, 0.014, 0.013, 0.012, 0.011, 0.01, 0.009, 0.008, 0.0075, 0.0072, 0.0065, 0.0071, 0.0057, 0.0055, 0.0044, 0.0044, 0.0033, 0.0033, 0.0032, 0.0029\}. \quad (6)$$

$$h_B = \{0.069, 0.1, 0.11, 0.098, 0.08, 0.06, 0.05, 0.04, 0.038, 0.032, 0.028, 0.024, 0.021, 0.019, 0.017, 0.015, 0.014, 0.013, 0.0118, 0.0108, 0.01, 0.0092, 0.0086, 0.008, 0.0075, 0.007, 0.0066, 0.0062, 0.0058, 0.0055, 0.0052, 0.00498, 0.00474, 0.00451, 0.00429, 0.0041, 0.0039, 0.0037, 0.0036, 0.0034, 0.0037, 0.0034, 0.0029, 0.0028, 0.0028, 0.0025, 0.0023, 0.0023, 0.002, 0.0017\}. \quad (7)$$

The impulse responses (6) and (7) are denoted Channel-A and Channel-B, respectively. Note that Channel-A and Channel-B span over $L = 30$ and $L = 50$ symbols, respectively.

III. IMPLEMENTATION

A binary information stream \mathbf{u} is firstly encoded by an Error Correcting Code (ECC) into a code word in rate R bit/symbol. In every time step n , the precoder maps $m = \log_2(Q)$ coded bits $b_n^m \triangleq (b_{n0}, b_{n1}, \dots, b_{n(m-1)})$ to a symbol x_n that satisfies a peak power constraint $p_n \leq \gamma$. To do so, the precoder firstly calculates the forbidden symbols for transmission at step n (symbols that would yield $p_n > \gamma$) according to the *channel state* s_n , where s_n is defined as the last $L - 1$ transmitted symbols $(x_{n-1}, x_{n-2}, \dots, x_{n-L+1})$. The sets of the forbidden and non-forbidden symbols are denoted by \mathbf{F} and $\overline{\mathbf{F}}$, respectively, where $\mathbf{F} \cap \overline{\mathbf{F}} = \emptyset$ and $\mathbf{F} \cup \overline{\mathbf{F}} = \mathbf{X}$. The calculation of \mathbf{F} is preformed according to (8), and $\overline{\mathbf{F}} = \{x \in \mathbf{X} : x \notin \mathbf{F}\}$.

$$\mathbf{F} = \left\{ x \in \mathbf{X} : \left| h_0 x + \sum_{i=1}^{L-1} h_i x_{n-i} \right|^2 > \gamma \right\} \quad (8)$$

Let us define the indicator vector $\mathbf{A} = (A_0, A_1, \dots, A_{Q-1})$ of the constellation \mathbf{X} as

$$A_i = \mathbb{1}_{\mathbf{F}}(x_i) = \begin{cases} 0, & x_i \in \mathbf{F} \\ 1, & x_i \in \overline{\mathbf{F}}, i = 0, 1, \dots, Q - 1 \end{cases} \quad (9)$$

According to a mapping table \mathbf{T} and the set \mathbf{A} in time step n , the bits b_n^m are uniquely map to a symbol $x_n \in \overline{\mathbf{F}}$. Note, the size of \mathbf{T} is 2^Q -by- Q (it does not depend on the channel length L). The precoder operation is summarized by the block diagram illustrated in Fig. 2.

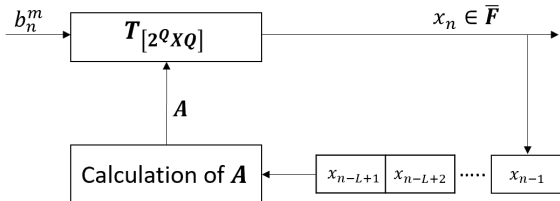


Figure 2: The precoding process.

The mapping table \mathbf{T} is constructed according to the following. If $\mathbf{F} = \emptyset$, $\overline{\mathbf{F}} = \mathbf{X}$ and the symbols bit labeling is the Gray labeling. Otherwise, all the bit labels of the symbols in \mathbf{F} cannot be used, and should be assigned to a corresponding symbols from $\overline{\mathbf{F}}$. Each label from \mathbf{F} should be assigned to a symbol from $\overline{\mathbf{F}}$ such that the hamming distance between the labels is minimal. In case of several choices of symbols from $\overline{\mathbf{F}}$, with the same minimal hamming distance, the symbol with the lowest Euclidean distance is chosen. The different bits among the common labels of a symbol are equivalent to erasure (could be zero or one since they are unknown to the receiver). The mapping table \mathbf{T} of a 4-PAM constellation, $\mathbf{X} = (-3, -1, 1, 3)$, is presented in Table I. The row index is the decimal representation of the binary set \mathbf{A} (i.e., if for

example $\mathbf{A} = (0, 1, 1, 1)$ and $b_n^m = (1, 1)$, the transmitted symbol is $x_n = \mathbf{T}_{73} = 3$).

	10	00	01	11
0	-	-	-	-
1	3	3	3	3
2	1	1	1	1
3	3	1	1	3
4	-1	-1	-1	-1
5	-1	-1	3	3
6	-1	-1	1	1
7	-1	-1	1	3
8	-3	-3	-3	-3
9	-3	-3	3	3
10	-3	-3	1	1
11	-3	-3	1	3
12	-3	-1	-1	-3
13	-3	-1	-1	3
14	-3	-1	1	1
15	-3	-1	1	3

Table I: Mapping table \mathbf{T} of a 4-PAM constellation.

The signal x^N at the precoder output is a Markov process. The Q^{L-1} distinct states of the Markov process are indexed by $i \in \mathbb{Z}$, $i = 0, 1, \dots, Q^{L-1} - 1$. Since $\Pr(s_n = j | s_{n-1} = i) = \Pr(j|i) \forall n$ then, the transmission is a stationary time-homogeneous Markov chain, and the transition between channel states is uniquely defined by a symbol $x_{ij} \in \mathbf{X}$ i.e., $\Pr(j|i) = \Pr(x_{ij}|i)$ where x_{ij} is the symbol that causes a transition from state i to state j .

At the receiver side we used a modified M-BCJR algorithm which computes online the states probabilities of the infinite-state Markov process. The M-BCJR algorithm [10] computes $\zeta_{ij,n} \triangleq \Pr(s_{n-1} = i; s_n = j; y^N)$ for all $0 < n \leq N - 1$ and for M states with the highest metrics at step $n - 1$. Next, m Log Likelihood Ratios (LLR), $\Lambda(b_{nl})$, $0 \leq l \leq m - 1$, are computed for each noisy symbol y_n according to

$$\Lambda(b_{nl}) = \log \left(\frac{\sum_{(i,j)} \sum_{x_{ij}:\hat{b}_l=0} \zeta_{ij,n} + \sum_{x_{ij}:\hat{b}_l=X} \zeta_{ij,n} \cdot \Pr(b_{nl} = 0)}{\sum_{(i,j)} \sum_{x_{ij}:\hat{b}_l=1} \zeta_{ij,n} + \sum_{x_{ij}:\hat{b}_l=X} \zeta_{ij,n} \cdot \Pr(b_{nl} = 1)} \right) - \Lambda^e(b_{nl}) \quad (10)$$

where the bit label of the symbol x_{ij} is denoted by \hat{b}^m and the ambiguous bits in the bit label are denoted by X . The bit probabilities $\Pr(b_{nl} = 0)$ and $\Pr(b_{nl} = 1)$ are calculated from $\Lambda^e(b_{nl})$, which is the extrinsic LLR from the code decoder. The calculation (10) requires, for each x_{ij} , both \hat{b}^m and the trellis branch probability $\Pr(x_{ij}|s = i)$. In uniform transmission, $\Pr(x_{ij}|s = i) = 1/Q \forall i, j$ and the symbols bit label is the Gray labeling in all states. However, in the suggested shaping scheme, $\Pr(x_{ij}|s = i)$ and \hat{b}^m depend on the state i , γ , and h^L . Calculation of these metrics is preformed according to the process illustrated in Fig. 3.

The LLR values Λ^{mN} at the BCJR output can be used as an a priory input to a ECC decoder. In each iteration, the decoder produces extrinsic LLR values $(\Lambda^e)^{mN}$ which are used as an a priory input to the BCJR module, which in turn calculates new extrinsic LLRs which are sent back to the code decoder.

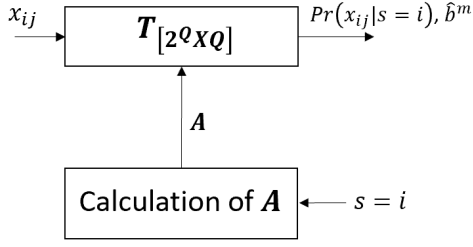


Figure 3: Trellis branch probability online calculation process.

After a pre-determined number of iterations has reached, the bit estimations \hat{u} are determined by performing hard decision on the decoder LLR values $(\Lambda^e)^{m,N}$. Initially, all $(\Lambda^e)^{m,N}$ are set to 0.

IV. THEORETICAL ANALYSIS

This section aims to study the achievable theoretical gains using shaping. In Section IV-A we derive a Lower-Bound (LB) on the SNDR given rate and TSTNR. It is well known that in this case the optimal one-dimensional symbols distribution is Gaussian. We optimized the Power Spectral Density (PSD) of the Gaussian distribution such that the achievable rate is maximized. This LB can be used for upper-bounding the SNDR gain, by comparing between the LB and the SNDR of a flat PSD (i.i.d distribution) at a given rate. In Section IV-B we estimate the receiver PAPR of a peak constrained transmission. We then use this estimation, together with the UB on the SNDR gain, to derive the theoretical shaping gain.

A. Upper Bound for Infinite Constellation

The channel capacity can be tightly approximated by $C = \lim_{N \rightarrow \infty} C_N$ [11] where

$$C_N \triangleq \frac{1}{2N} \sum_{i=0}^{N-1} \log \left(1 + \frac{2q_i |H_i|^2}{N_A + N_0} \right), \quad (11)$$

q^N are the energy spectral components of a Gaussian input process g^N , and H^N is N -points Discrete Fourier Transform (DFT) of the channel impulse response h^L . UB on the achievable rate given SNDR and TSTNR is found by optimizing the channel capacity (11) under the following constraints

$$\begin{aligned} \frac{1}{N} \sum_{i=0}^{N-1} q_i |H_i|^2 &\leq K \\ \frac{1}{N} \sum_{i=0}^{N-1} q_i &\leq P \end{aligned} \quad (12)$$

where $K, P \in \mathbb{R}_{\geq 0}$ are the constraints on receiver and transmitter average power, respectively.

We determine the maximum of C_N subject to the constraints (12) by introducing Lagrange multipliers (α, β) , $\alpha, \beta \geq 0$, and find the maximum of

$$\begin{aligned} J = & \sum_{i=0}^{N-1} \log \left(1 + \frac{2q_i |H_i|^2}{N_A + N_0} \right) - \alpha \left(\sum_{i=0}^{N-1} q_i |H_i|^2 - K \right) \\ & - \beta \left(\sum_{i=0}^{N-1} q_i - P \right) \end{aligned} \quad (13)$$

We get

$$\frac{\partial J}{\partial q_i} = \frac{2|H_i|^2}{2q_i |H_i|^2 + N_A + N_0} - \alpha |H_i|^2 - \beta = 0 \quad (14)$$

Solving (14) for q_i yields

$$q_i^o = \max \left[0, \frac{1}{\alpha |H_i|^2 + \beta} - \frac{N_A + N_0}{2|H_i|^2} \right] \quad (15)$$

Capacity is achievable if the input sequence g^N is a Gaussian process with energy spectral components $(q^o)^N$ and the multipliers α and β are chosen such that the constraints (12) are satisfied. Since we are interested in $(q^o)^N$ that yields the highest capacity for a given SNDR and TSTNR values, we optimized the capacity (11) with respect to K , while TSTNR and SNDR are kept constants i.e.,

$$C_o = \max_K \left(C_N |_{(SNDR, TSTNR)} \right) \quad (16)$$

The value of K that maximized (16) is denoted as K_o .

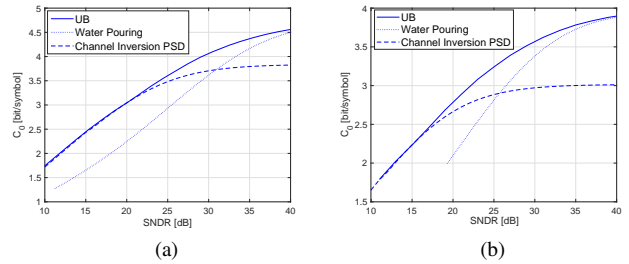


Figure 4: UB on the achievable rate for Channel-A. (a) TSTNR 45 dB. (b) TSTNR 40 dB.

The UB expression (15) can be divided to three regions, (a) $N_A \gg N_0$, (b) $N_A \ll N_0$, and (c) $N_A \approx N_0$. In the region $N_A \gg N_0$, N_0 has a negligible influence on the total noise power. The optimization process (16) therefore yields low K_o value. The reason is that in low K value, the constraint on the transmitted average power P is not effective since it is already satisfied. Hence, the optimal solution is to invert the channel, which is obtained from (15) by setting $\beta = 0$. The Lagrange multiplier α is chosen such that the average power constraint at the receiver is kept. In the region $N_A \ll N_0$, N_A has a negligible influence on the total noise. Since N_0 is constant, the optimization process (16) yields high K value. However, the receiver power constraint is not effective in case where K is higher than the average power that would have been obtained at the receiver without any constraint (as it is

already met). The optimal solution is therefore reduced to the well-known water-pouring solution, which is obtained from (15) by setting $\alpha = 0$. The Lagrange multiplier β is chosen such that the average power constraint at the transmitter is kept. In the region $N_A \approx N_0$, both noises influences on the total noise power thus, the optimal solution is given by (15). As an example, the channel capacity (16), under the constraints (12), was calculated over Channel-A for TSTNR 45 dB and 40 dB. UB on the rate (or, equivalently, LB on the SNDR) in these TSTNR values is illustrated in Fig. 4(a) and Fig. 4(b), respectively.

B. Estimation of Receiver PAPR

In an un-shaped transmission, the one-dimensional distribution of each sample at channel output, according to CLT, approaches the Gaussian distribution. In a peak constrained transmission, this distribution could be therefore approximated by the Truncated Gauss (TG) distribution in the region $[-\sqrt{\gamma}, \sqrt{\gamma}]$. The probability density function of such distribution is

$$f(r) = \frac{\exp\left(-r^2/2\sigma^2\right)}{\sqrt{2\pi\sigma^2}(1 + \operatorname{erf}(\sqrt{\gamma}/2\sigma^2))} \quad (17)$$

γ	Channel-A		Channel-B	
	TG Gauss	Simulation	TG Gauss	Simulation
-16 dB	4.89 dB	4.9 dB	4.95 dB	5.15 dB
-14 dB	4.96 dB	5.27 dB	5.06 dB	5.3 dB
-12 dB	5.07 dB	5.3 dB	5.24 dB	5.42 dB
-10 dB	5.24 dB	5.56 dB	5.51 dB	5.63 dB
-8 dB	5.52 dB	5.75 dB	5.95 dB	6.1 dB
-6 dB	6 dB	6.07 dB	6.65 dB	6.85 dB
-4 dB	6.65 dB	6.63 dB	7.73 dB	8.09 dB
-2 dB	7.7 dB	7.58 dB	9.15 dB	9.6 dB
0 dB	10.08 dB	10.03 dB	11.17 dB	11.4 dB

Table II: PAPR of TG Gauss and online shaping scheme.

and its PAPR is

$$\operatorname{PAPR}_{TG} = \frac{\gamma}{K_{TG}} \quad (18)$$

where

$$K_{TG}(\gamma) = \sigma^2 - \operatorname{erf}\left(\sqrt{\gamma}/2\sigma^2\right)^{-1} \sqrt{\frac{2\gamma\sigma^2}{\pi}} \exp(-\gamma/2\sigma^2) \quad (19)$$

is the average power and σ^2 is the un-shaped (i.i.d) received signal average power i.e., $\sigma^2 = \sum_{i=0}^{L-1} h_i^2$.

A comparison between (18) and the PAPR which yields the online shaping scheme at Channel-A and Channel-B outputs is summarized by Table II, for different γ values. It can be seen that indeed (18) approximates well the practical PAPR achieved by the online shaping scheme.

C. Theoretical Shaping Gain

The PAPR gain in a specified γ is found by comparing (18) to receiver PAPR of uniform 4-PAM transmission. The

SNDR gain is found in a specified γ , rate and TSTNR, by comparing the theoretical SNDR of an un-shaped (i.i.d) Gaussian input distribution and the theoretical SNDR achieved by constraining the receiver power to $K = K_{TG}(\gamma)$. The relationships between the theoretical shaping gains and γ in rate 1.8 bits/symbol over Channel-A are demonstrated in Fig. 5(a) and Fig. 5(b), for TSTNR of 40 dB and 34 dB, respectively. It can be seen that the maximal theoretical shaping gains in these cases are 11.65 dB and 8.83 dB, respectively. The maximal theoretical shaping gains in rate 1.8 bits/symbol over Channel-A, and the corresponding γ values, are summarized in Table III for several TSTNR values.

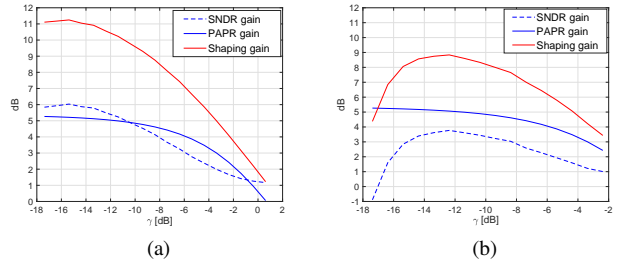


Figure 5: Relationship between theoretical gains and γ in rate 1.8 bits/symbol over Channel-A. (a) TSTNR 40 dB. (b) TSTNR 34 dB.

TSTNR	γ	G_T
45 dB	-15 dB	12.34 dB
40 dB	-15 dB	11.25 dB
37 dB	-13 dB	9.75 dB
34 dB	-12 dB	8.83 dB
31 dB	-10 dB	7.71 dB
29 dB	-7 dB	6.5 dB

Table III: Theoretical shaping gains in rate 1.8 bits/symbol over Channel-A for several TSTNR values.

V. SIMULATION RESULTS

The shaping was applied over 4-PAM and 8-PAM constellations with code rates 0.9 and 0.6, respectively. Hence, the data rate in all systems is $R = 1.8$ bits/symbol or, equivalently, 200 Gbps for Channel-A and 400 Gbps for Channel-B.

The code used with all schemes is a standard turbo encoder [12], made up of two elementary encoders with memory size 4 and the same generator polynomial 37-23 (octal number 37 represents the feed-forward connections and 23 the feedback connections). This code is known to be an optimal code with memory size 4 for various turbo-code rates [13]. At the receiver, the number of survivors states we used in the M-BCJR module, in all systems, was $M = 16$ states per time step. The turbo decoding ran for maximum 12 iterations on block length of 4096 information bits. The shaped systems are compared to uniform 4-PAM transmission with TE at the receiver, over the same channel.

The resulting PAPR distributions at Channel-A output and the BER curves are presented in Fig. 6(a) and Fig. 7(a) respectively, for TSTNR 40 dB. As was shown in Fig. 5(a),

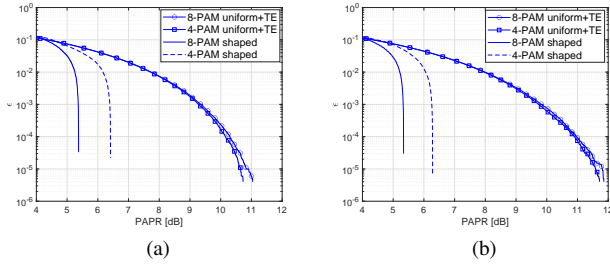


Figure 6: PAPR distributions at the channel output for TSTNR 40 dB and rate 1.8 bits/symbol. (a) Channel-A. (b) Channel-B.

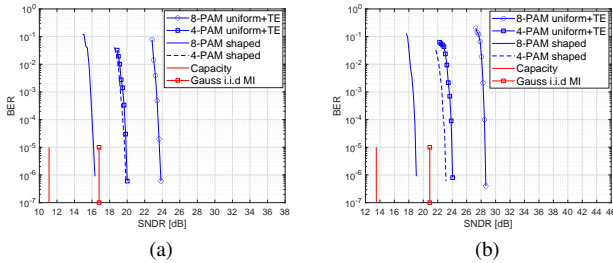


Figure 7: BER Vs. SNDR for TSTNR 40 dB and rate 1.8 bits/symbol. (a) Channel-A. (b) Channel-B.

the maximal gain is achieved in γ -15 dB. However, since for practical implementation the shaping was applied over Q -point constellation rather than infinite set of points, the optimal BER performance was achieved in γ of -14 dB and -3.9 dB for shaped 8-PAM and shaped 4-PAM systems, respectively. The SNDR at which BER 10^{-6} is reached, the PAPR at Channel-A output and the required ENOB are summarized in Table IV. It can be seen that the shaped 8-PAM and 4-PAM systems achieve, overall shaping gains of 8.55 dB and 4.05 dB, respectively, compared to uniform 4-PAM transmission with TE. These gains translates to ENOB gain of 1.43 bit and 0.68 bit, respectively. Comparing the SNDR gain to the theoretical SNDR gain indicates that the online shaping scheme suffers from loss of 1.98 dB.

System	PAPR 10^{-4}	SNDR 10^{-6}	ENOB
8-PAM uniform + TE	10.35 dB	23.85 dB	4.9 bit
4-PAM uniform + TE	10.13 dB	20.02 dB	4.23 bit
8-PAM shaped	5.3 dB	16.3 dB	2.8 bit
4-PAM shaped	6.45 dB	19.65 dB	3.55 bit

Table IV: Rate 1.8 bits/symbol and TSTNR 40 dB over Channel-A, PAPR at channel output, SNDR and ENOB summary.

In the case of rate 1.8 bits/symbol over Channel-B and TSTNR 40 dB, the maximal gain was obtained when constraining the peak power, γ , to -17 dB. The resulting PAPR distributions and the BER curves are presented in Fig. 6(b) and Fig. 7(b), respectively. As before, the metrics of interest are summarized in Table V. It can be seen that the shaped 8-PAM and 4-PAM systems achieve overall shaping gains of 10.65 dB and 5.45 dB, respectively, compared to uniform 4-

PAM transmission with TE. These gains translates to ENOB gain of 1.78 bit and 0.91 bit, respectively.

System	PAPR 10^{-4}	SNDR 10^{-6}	ENOB
8-PAM uniform + TE	11 dB	28.3 dB	5.75 bit
4-PAM uniform + TE	10.95 dB	24 dB	5.03 bit
8-PAM shaped	5.3 dB	19 dB	3.25 bit
4-PAM shaped	6.4 dB	23.1 dB	4.12 bit

Table V: Rate 1.8 bits/symbol and TSTNR 40 dB over Channel-B, PAPR at channel output, SNDR and ENOB summary.

VI. CONCLUSION

A novel online shaping technique for PAPR reduction at the output of high-speed wireline channels has presented. The technique is effective to reduce the large ADC dynamic range requirement and by that the required ENOB, such that an overall gain is achieved compared to uniform transmission with TE at the receiver. Theoretical analysis which provides a LB on the SNDR and theoretical shaping gains has derived as well. In data rate of 200 Gbps and 400 Gbps, an overall ENOB gains was demonstrated to be up to 1.43 bit and 1.78 bit, respectively, compared to a uniform 4-PAM transmission with TE at the receiver side.

REFERENCES

- [1] D. Sadot, G. Dorman, A. Gorshtein, E. Sonkin, and O. Vidal, "Single channel 112 Gbit/sec PAM4 at 56Gbaud with digital signal processing for data centers applications," *Opt. Exp.*, vol. 23, no. 2, pp. 991–997, Jan.2015.
- [2] "IEEE Standard for Terminology and Test Methods for Analog-to-Digital Converters," IEEE Standard 1241-2010
- [3] R.F.H. Fischer, W. Gerstacker, J.B. Huber, "Dynamics Limited Precoding, Shaping, and Blind Equalization for Fast Digital Transmission over Twisted Pair Lines," *IEEE Journal on Selected Areas in Communications*, vol. 13, no. 9, pp. 1622-1633, December 1995.
- [4] M. Tomlinson, "New automatic equaliser employing modulo arithmetic," *Electron. Lett.*, vol. 7, no. 5, pp. 138–139, 1971.
- [5] S. Hall and H. Heck, "Advanced Signal Integrity for High Speed Digital Designs," WILEY, 2009.
- [6] O. Levi, D. Raphaeli, Y. Tate, "A Novel Shaping Scheme for PAPR Reduction in Single-Carrier Modulation," *IEEE Trans. Commun.*, vol. 66, no. 9, pp 4222-4233, Sep. 2018.
- [7] M. Tuchler, R. Koetter, and A. C. Singer, "Turbo Equalization: Principles and New Results," *IEEE Trans. Commun.*, vol. 50, no.5, pp. 754767, May 2002.
- [8] Kester, Walt, ed. 2004. "Analog-Digital Conversion," Analog Devices, Inc.
- [9] W. Guo, J. Lin, C. Lin, T. Huang, R. Wu, "Fast methodology for determining eye-diagram characteristics of lossy transmission lines," *IEEE Trans. Adv. Packag.*, vol.32, no.1, pp 175-183, Feb. 2009.
- [10] V. Franz and J. Anderson, "Concatenated decoding with a reduced-search BCJR algorithm," *IEEE J. Select. Areas Commun.*, vol. 16, no. 2, pp. 186–195, Feb. 1998.
- [11] W. Hirt and J. L. Massey, "Capacity of the discrete-time Gaussian channel with intersymbol interference," *IEEE Trans. Inform. Theory*, vol. 34, no. 3, pp. 380-388, May 1988.
- [12] C. Berrou, A. Glavieux, and P. Thitimajshima, "Near optimum error correcting coding and decoding: Turbo-codes," *IEEE Trans. Commun.*, vol. 44, no. 10, pp. 1261–1271, Oct. 1996.
- [13] S. Benedetto, R. Gallardo, and G. Montorsi, "A search for good convolutional codes to be used in the construction of turbo codes," *IEEE Trans. Commun.*, vol. 46, no. 9, pp. 1101–1105, Sep. 1998.